HHS Public Access

Author manuscript

Biomaterials. Author manuscript; available in PMC 2016 March 21.

Published in final edited form as:

Biomaterials. 2013 April ; 34(11): 2641–2654. doi:10.1016/j.biomaterials.2012.12.048.

Decellularized musculofascial extracellular matrix for tissue engineering

Lina Wang, **Joshua A Johnson**, **David W. Chang**, and **Qixu Zhang***

Department of Plastic Surgery, The University of Texas MD Anderson Cancer Center, Houston, TX 77030, USA

Abstract

Ideal scaffolds that represent native extracellular matrix (ECM) properties of musculofascial tissues have great importance in musculofascial tissue engineering. However, detailed characterization of musculofascial tissues' ECM (particularly, of fascia) from large animals is still lacking. In this study, we developed a decellularization protocol for processing pig composite musculofascial tissues. Decellularized muscle (D-muscle) and decellularized fascia (D-fascia), which are two important components of decellularized musculofascial extracellular matrix (DMM), were comprehensively characterized. D-muscle and D-fascia retained intact three-dimensional architecture, strong mechanical properties, and bioactivity of compositions such as collagen, laminin, glycosaminoglycan, and vascular endothelial growth factor. D-muscle and D-fascia provided a compatible niche for human adipose-derived stem cell integration and proliferation. Heterotopic and orthotopic implantation of D-muscle and D-fascia in a rodent model further proved their biocompatibility and myogenic properties during the remodeling process. The differing characteristics of D-muscle from D-fascia (e.g., D-muscle's strong pro-angiogenic and pro-myogenic properties vs. D-fascia's strong mechanical properties) indicate different clinical application opportunities of D-muscle vs. D-fascia scaffolds. DMM comprising muscle and fascia ECM as a whole unit can thus provide not only a clinically translatable platform for musculofascial tissue repair and regeneration but also a useful standard for scaffold design in musculofascial tissue engineering.

Keywords

Decellularization; Skeletal muscle; Fascia; Extracellular matrix; Scaffold; Adipose-derived stem cell

1. Introduction

Significant soft tissue loss caused by trauma or tumor removal currently requires autologous tissue transplantation. This type of surgical reconstruction, which utilizes musculofascial tissue from local or distant sites, is associated with donor sites morbidity, functional loss, and volume deficiency. With developments in the fields of biomaterials and stem cells, new

*Corresponding author: Qixu Zhang, MD, PhD, Plastic Surgery Department, The University of Texas M.D. Anderson Cancer Center, 8010 El Rio Street, Unit 602, Houston, TX 77054-4104. Tel: +1 713 563 7565; fax: +1 713 563 0321. qzhang5@mdanderson.org (Q. Zhang).

biological scaffolds and techniques have become potential alternative approaches for soft tissue repair and regeneration [1–6]. The utilization of biologically engineered implants for reconstructive surgery could provide a more accessible tissue source and avoid the limitation of autologous tissue grafts. For the design of three-dimensional (3D) scaffolds as implants or carriers for stem cell therapy, standards for 3D scaffolds that can mimic host extracellular matrix (ECM) are needed. According to the plastic surgery rule that 'replace with alike', the scaffold designs for different tissues should be based on those specific tissues. Germane to our interest, ideal scaffolds that can represent native ECM of musculofascial tissues have great importance in musculofascial tissue engineering. However, information on native musculofascial tissues' ECM (particularly, of fascia) from large animals is still limited.

Decellularization, a technique to remove cell components and maintain the ECM of tissues, provides a means of studying the native ECM [1, 7]. This process is supposed to provide a 3D microenvironment that mimics the natural niche for cell growth and function. This technique has been applied to process different types of tissues, such as heart, liver, skin, fat, peripheral nerve and muscle [1, 7–16]. Studies have reported on decellularized muscle matrices from mice and rats and their application in repairing muscle defects in rat models [17–19]. However, these reports only provided information on muscle ECM from small animals, which do not accurately meet patients' needs in clinic. One recent study prepared decellularized matrix from pig muscles to repair muscle defects in a rat model. However, the decellularized pig muscle matrix was made into a gel format in that study [20]. Comprehensive characterization of the intact muscle ECM derived from large animals, such as pigs, is still not available.

Besides muscles, fascia is another important component in musculofascial tissues. In reconstructive surgery, both fascia and muscle are treated together as an intact unit in musculofascial defect repair. For design and fabrication of scaffolds that could meet clinical needs and translate from bench to bed, ideal scaffolds for engineering musculofascial tissues should recapitulate ECM properties of both fascia and muscle. Current reports all focus on the decellularizing skeletal muscles alone [19]. Little information on decellularized fascia is available.

The present study aimed to establish a platform for musculofascial tissue engineering through a decellularization approach for large animal (i.e. pig) musculofascial tissues, which could be potentially translated to clinical application and could provide scaffold-design standards for musculofascial tissue engineering. Following decellularization principles and based on currently existing protocols, we developed a decellularization protocol for processing pig musculofascial tissues to maintain natural ECM architecture and biochemical compositions. Decellularized muscle (D-muscle) and decellularized fascia (D-fascia), which are two important components of decellularized musculofascial matrix (DMM), were comprehensively characterized with respect to 3D architecture, biomolecular patterning, and bioactivity of compositions. Biocompatibility of D-muscle and D-fascia was tested by human adipose-derived stem cell (hASC) integration. D-muscle and D-fascia were then implanted in a rodent model to evaluate the *in vivo* response, biocompatibility, and remodeling properties. Furthermore, D-muscle was applied to repair muscle defects in a rodent model. This study may lead to a platform as well as a standard for designing and

fabricating 3D scaffolds that mimic the *in vivo* microenvironment for musculofascial tissue repair and regeneration.

2. Materials and methods

2.1. Decellularization of musculofascial tissue

All procedures were approved by the Institutional Animal Care and Use Committee of The University of Texas MD Anderson Cancer Center and met all requirements of the Animal Welfare Act.

A euthanized domestic pig (100kg) was used as a donor animal. Tissue was harvested and processed under sterile conditions. Briefly, the anterior abdominal wall was used as a surgical field. A paramedian incision was made to expose the external oblique muscles. Dissect anterior rectus fascia underneath the external oblique muscles, and identify rectus abdominal muscles. Then the anterior rectus fascia and rectus abdominal muscle sample were harvested (Supplementary Figure 1). Tissues were cut into 4×2×0.5-cm pieces, stored in saline on ice, and delivered to the lab for further processing within 4 h after harvest. Native tissues were evaluated immediately after samples were delivered to the lab.

All decellularization steps were carried out at room temperature (except where indicated) with agitation (120 rpm). First, samples were frozen at −80 °C and thawed at room temperature for 3 cycles and then washed in ultrapure water for 2 days. These samples were then treated with 0.5M NaCl for 4 h, followed by 1M NaCl for 4 h, and washed in ultrapure water overnight; this procedure was repeated once. After being treated with 0.25% trypsin/EDTA at 37 °C for 2 h, the samples were washed in DI water for 1 h. The samples were treated with 1% Triton X-100 for 5 days (one change every day), processed with DNAase at 37°C for 3 h, washed in ultrapure water for 2 days, and rinsed in PBS for 1 day. The samples were then stored at 4 °C until use.

2.2. Immunohistochemical analysis

Native muscle, native fascia, D-muscle, and D-fascia were fixed in 10% formalin, embedded in paraffin, and sectioned into 5-μm slices. Sections were deparaffinized, rehydrated, and washed in distilled H_2O. Slides underwent histological hemoatoxylin and eosin (H&E) and Masson Trichrome staining. For immunohistochemical staining, slides were placed in 95°C antigen retrieval citrate buffer (Biogenex, Fremont, CA) in a steamer for 10 minutes. Endogenous peroxidases were blocked by incubation with Peroxide Block (Innogenex, San Ramon, CA), and nonspecific binding was blocked with normal goat serum (Vector Laboratories, Burlingame, CA). Sections were incubated overnight with primary antibody at 4°C (anti-laminin, Abcam, Cambridge, MA; anti-VEGF, Oncogene Science, Cambridge, MA; and anti-MHC-1, Abcam, Cambridge, MA). After washing, biotinylated secondary antibody was applied for 30 minutes, followed by treatment with streptavidin-horseradish peroxidase complex (Vectastain ABC kit, Vector Laboratories), diaminobenzidine (DAB) solution (DAB kit, Vector), and counterstaining with hematoxylin. Slides were dehydrated, mounted, and imaged using an Olympus IX71 microscope (Olympus, Center Valley, PA).

2.3. DNA assessment and quantification

Slides cut from paraffin-embedded samples underwent DAPI staining to show cell removal; an absence of staining indicates absence of DNA and thus cells. Cell removal was further quantified by measuring nucleic acid concentration with the Quant-iT™ PicoGreen® dsDNA assay kit (Molecular Probes, Eugene, OR). Native tissues and decellularized samples were digested in 1 mg/mL papain (Sigma, St. Louis, MO) at 60 °C for 48 hours. Samples were centrifuged at 12000 rpm at 4 °C for 10–15 minutes. Supernatants from samples were measured for fluorescence intensity using a VersaFluor™ spectrofluorometer (Bio Rad Laboratory Inc., Hercules, CA), and measured DNA quantity was normalized to the initial dry weight of the tissue.

2.4. Sulfated glycosaminoglycan (GAG) content

Sulfated GAG contents of native tissues and decellularized samples were quantified using an Alcian blue colorimetric assay kit (sGAG Dye Binding Assay, ALPCO, Salem, NH). Samples were lyophilized and papain-digested followed by incubation with Alcian blue dye. Absorbance of the samples at 600–620nm was measured with a Beckman Coulter DU730 UV/Vis Spectrophotometer using chondroitin sulfate (Sigma, St. Louis, MO) as the standard. GAG content was normalized to the initial dry weight of the samples.

2.5. Scanning electron microscopy (SEM)

Native tissues and decellularized samples were frozen at −80°C and dried through lyophilization. Cells on decellularized samples were fixed with 2% paraformaldehyde and 3% glutaraldehyde in PBS for 1 h and 0.1M cacodylate buffer (three times for 5 min each). This was followed by postfixing with 1% OsO_4 in 0.1M sodium cacodylate buffer for 1 h and rinsing in cacodylate buffer three times (5 min each). The samples were then dehydrated in 35, 50, 70, 80, 95, and 100% ethanol successively for 10 min each and dried in hexamethyldisilazane (HMDS, Sigma, St. Louis, MO). These dry samples were coated under vacuum using a Balzer MED 010 evaporator (Technotrade International, Manchester, NH) with platinum alloy for a thickness of 25 nm, and immediately flash carbon coated under vacuum. Samples were examined in a JSM-5910 scanning electron microscope (JEOL, USA, Inc., Peabody, MA) at an accelerating voltage of 5 kV. Cell morphology (e.g. perimeter, area, roundness and elongation) was measured using image-processing software Simple PCI (Compix Inc., Cranberry Township, PA). Roundness is defined as $4*\pi*\text{area}/(\text{perimeter})^2$. Elongation is defined as length/width.

2.6. Mechanical test

The mechanical properties of native tissues and decellularized samples were determined by uniaxial tensile testing using the Bose EnduraTEC EL3200 system which has high sensitivity and wide load cell capacity (250N load cell). Stress vs. strain curves were collected. Ultimate tensile strength (UTS), elastic modulus (E), and strain at failure were determined using these curves.

2.7. Aortic ring assay

D-muscle and D-fascia were ground into a fine powder and then incubated with EGM™ endothelial growth medium (Lonza, Walkersville, MD) at 37°C for 72 hours with agitation. After centrifugation, the supernatant was saved as conditioned medium for future use. An aortic ring assay was applied to test the effects of D-muscle-conditioned media and D-fascia-conditioned media on angiogenesis [21, 22]. The rat thoracic aorta was obtained from 8- to 10-week-old male Fischer 344 rats (Harlan Laboratories, Indianapolis, IN). The aorta was sectioned into 1-mm-thickness rings. Those aortic rings were then immersed in 25 μl rat-tail collagen type I (BD Biosciences, San Diego, CA) and incubated at 37°C for 30 min while the collagen solution transformed into a gel. Aortic rings embedded in collagen gels were treated with D-muscle conditioned EGM, D-fascia conditioned EGM, or EGM alone. Phase contrast images were taken for these samples on days 3, 7, and 9 using an Olympus IX70 microscope before and after hemotoxylin staining. Cell outgrowth and migration from the rings were analyzed by ImageJ software. On day 9, aortic rings with outgrowth of cells and branches were immunostained with mouse monoclonal primary antibody to CD31 (1:200, AbD SeroTec, Raleigh, NC) and rabbit monoclonal primary antibody to α-smooth muscle actin (1:200, Abcam, Cambridge, MA), followed with goat anti-mouse DyLight 488 (1:500, Jackson Immuno Research Laboratories, West Grove, PA) and goat anti-rabbit Dylight 594 (1:500, Jackson Immuno, West Grove, PA), respectively. DAPI (1:5000, Molecular Probes, Eugene, OR) was used to stain cell nuclei. Images were viewed with an Olympus IX81confocal fluorescence microscope.

2.8. hASC culture

All procedures were conducted under institutional review board approval and in accordance with research guidelines at the University of Texas MD Anderson Cancer Center. Adipose tissue samples (subcutaneous adipose tissue in abdominal wall area) were collected from patients undergoing reconstructive surgery. These tissues are usually discarded after surgery. These samples were kept on ice and delivered to the lab for further processing within 4 h after excision. Adipose tissues were minced and digested using 0.075% type IA collagenase (Sigma, St. Louis, MO) for 2 hours in sterile PBS buffer. Digested fat was filtered and centrifuged to obtain a cell pellet. Red blood cell lysis buffer (Biolegend Inc., San Diego, CA) was used to further purify the obtained the cell pellet. Obtained ASCs were grown in α-minimum essential medium (Mediatech, Manassas, VA) containing 10% fetal bovine serum (Invitrogen, Carlsbad, CA), 2mM L-glutamine, 100μg /ml penicillin, and 100 μg/mL streptomycin (Invitrogen, Carlsbad, CA) and plated out in T-25 culture flasks (BD, San Diego, CA). Flasks were maintained at 37°C in a 5% CO_2 humidified incubator.

2.9. Evaluation of hASCs integration with D-muscle and D-fascia

hASCs within 3 passages were harvested and plated onto D-muscle and D-fascia samples at a density of 1×10^5 cells/cm^2. ASCs were stained with calcein AM (Biotium, Hayward, CA). Briefly, cells were washed with PBS three to five times. Then cells were exposed to 2 μM calcein AM in PBS and incubated for 30 min at 37 °C before the staining solution was replaced. Samples were washed with PBS 3 times before viewing under a confocal microscope. Samples were examined on days 1, 3, and 7 after cell seeding.

Cell-substrate interaction was studied by immunostaining of integrins at day 1 of integration. hASCs were stained with rabbit monoclonal primary antibody to β_3 (1:200, Abcam, Cambridge, MA) and mouse monoclonal primary antibody to α_5 (1:200, Abcam, Cambridge, MA), followed by goat anti-rabbit DyLight 488 (1:500, Jackson Immuno, West Grove, PA) and goat anti-mouse DyLight 488 (1:500, Jackson Immuno, West Grove, PA), respectively. Samples were imaged with an Olympus IX81confocal fluorescence microscope.

2.10. In vivo test of D-muscle and D-fascia

Male 8- to 10-week-old Fischer 344 rats (Harlan Laboratories, Indianapolis, IN) were anesthetized and maintained with isoflurane (0.5–2%, 3–5 L/min) and oxygen. D-muscle and D-fascia samples were implanted subcutaneously on the backs of the rats (heterotopic implantation). For muscle defect repair, a 0.5 × 1 cm outer quadriceps muscle defect was created on the right side. D-muscle was implanted into the defect site (orthotopic transplantation). 6–0 Prolene sutures with a simple interrupted pattern were used to prevent movement of the construct from the recipient site. A second identical muscle defect was created and left unrepaired as a control. Animals were monitored for clinical signs of inflammation or rejection for 30 days and then euthanized (n=4).

Specimens were cut at the center of explants, and they were fixed in 10% formalin. Slides cut from paraffin embedded samples underwent H&E staining, Masson Trichrome staining, and immunohistochemical staining for CD68, CD80, CD163, CD31, and MyoD1 (all at 1:200, Abcam, Cambridge, MA). Positively stained cells were counted to evaluate the host immunological response and remodeling properties of the DMM.

2.11. Statistical analysis

Data were presented as mean ± standard deviation (s.d.). Data were analyzed using one-way analysis of variance (ANOVA) and Student t-test with SigmaStat. P values of less than 0.05 were considered significant.

3. Results

3.1. Confirmation of cell removal in D-muscle and D-fascia

Native muscle samples and native fascia samples underwent one cycle of the decellularization process. Supplementary Figure 2 and Figure 1(A) show typical images of muscle and fascia samples before and after decellularization process. No color change was observed in fascia samples after decellularization, while muscle samples turned from red-pink to white after processing. H&E staining revealed cell nuclei present in native tissues (Supplementary Figure 2) but absent in D-muscle and D-fascia (Figure 1(B)). A similar finding was observed with DAPI staining (Supplementary Figure 2 and Figure 1(C)). DNA content was significantly reduced from 0.11 ± 0.06 μg/mg dry weight in native muscle to 0.02 ± 0.01 μg/mg in D-muscle (n=3, $P<0.05$) and from 0.57 ± 0.30 μg/mg in native fascia to 0.02 ± 0.00 μg/mg in D-fascia (n=3, $P<0.05$) (Figure 1(D)). These results indicated that significant removal of cellular components had occurred in D-muscle and D-fascia samples.

3.2. 3D architecture and molecular composition in D-muscle and D-fascia

SEM was used to evaluate the 3D architecture of native muscle, D-muscle, native fascia, and D-fascia to confirm that the decellularization process did not alter ECM structures. Muscle fibers were observed in native muscle tissues (Supplementary Figure 3(A)) but had been removed in D-muscle samples (Figure 2(A)), leaving hollow and tubular structures. Nanofibrous structures from ECM were well maintained in D-muscle (Figure 2(A). Cells were observed within tissues in native fascia (Supplementary Figure 3(B)) but were absent in D-fascia samples (Figure 2(B)). The ECM structure seen in native fascia remained intact in D-fascia.

The major ECM components' spatial presence was assessed by immunohistochemical staining. Masson Trichrome staining indicated that tubular structures of D-muscle samples observed in SEM images (Figure 2(A)) were composed of collagen (Figure 3(A)). The major structure of D-fascia observed in Figure 2(B) was composed of collagen bundles (Figure 3(A)). These collagen bundles formed an oriented layered structure in fascial tissues. Another important biochemical molecule present in ECM is laminin, which plays an important role in mediating cell attachment. In native muscle tissues, laminin was distributed around muscle fiber bundles (Supplementary Figure 4(A)). After decellularization, the fibrous structures among collagen structures were stained positively for laminin (Figure 3(B)). Similar laminin distribution was noticed in native fascia (Supplementary Figure 4(A) and D-fascia (Figure 3(B)). VEGF plays an important role in angiogenesis/neovascularization. Immunohistochemical analysis indicated that VEGF was retained in D-muscle. VEGF staining was observed within small tubular structures (Supplementary Figure 4(B) and Figure 3(C)), which corresponded to the nanofibrous structures observed by SEM (Figure 2(A)). In D-fascia, VEGF staining was weakly positive. In native fascia, VEGF was only observed in limited areas among collagen bundles (e.g. around blood vessels), which suggested that native fascia may not be rich in VEGF. MHC-1, which acts as alloantigen and can provoke immune response in the recipient after transplantation, has been removed in D-muscle and D-fascia samples (Figure 3 (D)) as compared to native tissues (Supplementary Figure 4(C)). Quantification of GAG content showed a higher content in D-fascia samples (46.58±11.20 μg/mg dry weight) than in D-muscle samples (26.33±3.88 μg/mg dry weight) ($n=3$, $P < 0.05$).

3.3. Mechanical properties of D-muscle and D-fascia

Mechanical properties of D-muscle and D-fascia samples were measured by uniaxial tensile testing. Figure 4 shows a typical strain-stress curve from uniaxial tensile testing, and Table 1 summarizes these results. D-fascia presented significantly stronger UTS (4.02±1.49 MPa) and E (8.15±4.96 MPa) than did D-muscle (UTS = 1.32±0.85 MPa, E = 0.41±0.32 MPa) ($n=6$, $P<0.05$). However, D-muscle showed larger strain at failure (1.60±0.30) than D-fascia (0.65±0.19) ($n=6$, $P<0.05$) ($n=6$, $P<0.05$). UTS and E values did not change significantly from native fascia to D-fascia samples. However, UTS significantly increased for D-muscle as compared to native muscle ($n=6$, $P<0.05$).

3.4. D-muscle and D-fascia support ASC integration

hASCs were cultured on D-muscle and D-fascia samples. Live cell staining was utilized to demonstrate that D-muscle and D-fascia could support hASC survival. hASCs attached well to D-muscle and D-fascia after plating at day 1 (Figure 5(A)). When cultured *in vitro*, ASCs proliferated on both D-muscle and D-fascia samples from day 1 to day 3. Cells became confluent at day 7 on both D-muscle and D-fascia, and cell elongation was obvious at day 7. Cells elongated and oriented from day 3 to day 7 in culture (Figure 5(A)). Cell morphology was evaluated by SEM (Figure 5(B)). Quantitative analysis of cell morphology (i.e. cell spreading area, cell perimeter, elongation, and roundness) confirmed significant morphological changes of cells cultured on DMM from day 3 to day 7 (Table 2). For example, elongation of ASCs on D-fascia was 1.9 ± 1.1 at day 3 in culture, but increased to 13.0 ± 4.3 at day 7 in culture ($P<0.05$). Elongation of ASC on D-muscle was 2.3 ± 1.3 at day 3 in culture, but increased to 10.7 ± 5.0 at day 7 in culture ($P<0.05$). At day 3, ASCs on D-fascia differed from ASCs on D-muscle with respect to cell spreading area, perimeter, and roundness (Table 2). However, at day 7, only roundness differed for ASCs on D-muscle and D-fascia samples (Table 2).

ASC-scaffold interaction was further studied by evaluating integrin (i.e. α_5 or β_3) expression in hASCs cultured on D-muscle and D-fascia samples. hASCs cultured on 2D glass slides were used as controls for comparison. Figure 6 shows typical confocal images of hASCs cultured on a 2D glass slide, D-muscle, and D-fascia samples. Cells were stained for integrins α_5 and β_3. Similar integrin distribution patterns were observed for hASCs on 2D glass slides and on D-muscle and D-fascia (Figure 6). For example, integrin α_5 was distributed around the perimeter of cells cultured on 2D glass slides and on both D-muscle and D-fascia, while β_3 was observed around the nuclear region. Compared with 2D cultured hASCs, cells cultured on D-muscle and D-fascia appeared brighter when observed under the same settings (Figure 6).

3.5. Evaluation of pro-angiogenic properties of D-muscle and D-fascia

An aortic ring assay was utilized to test the effect of D-muscle and D-fascia on cell outgrowth from aortic rings and new vessel formation around aortic rings (Figure 7 (A)). Cell outgrowth was observed in all groups (control without conditioned media, D-muscle conditioned media, D-fascia conditioned media). Cells had expanded further at day 7 and day 9 than at day 3 ($n=3$, $P<0.05$) for all three groups (Figure 7 (B)). However, whereas there was no difference between the day 7 and day 9 measurements in the control group, in the D-fascia group and D-muscle groups, cell outgrowth distance increased significantly from day 7 to day 9 ($P<0.005$) (Figure 7 (B)). At day 3, there was no difference between the control group and the D-muscle group, but the D-fascia group showed significantly further distance than the other two groups ($P<0.005$). At day 7, there was no difference between the D-muscle and D-fascia groups, but both groups showed significantly further distance than the control group ($P<0.005$). At day 9, there was a significant difference among these three groups ($P<0.005$). In addition to cell outgrowth, new vessel formation was clearly observed in the D-muscle group but not in the control group or D-fascia group (Figure 7(A) and (C)). Vessel branches extending from the aortic ring in 3D collagen gels (Figure 7(C) and

Supplementary Video 1) were positive for both a smooth muscle marker (α-SMA) and an endothelial cell marker (CD31).

3.6. Evaluation of in vivo implanted D-muscle and D-fascia

D-muscle and D-fascia samples were implanted subcutaneously in Fischer 344 rats. Samples were harvested at day 30 and underwent histological analysis. H&E staining showed that implanted D-muscle and D-fascia were capsulated with uniform cell infiltration within the implanted samples (Figure 8(A)). Among all infiltrated cells in D-muscle and D-fascia samples, a portion was stained positively for CD68 and CD163 but negatively for CD80 (Figure 8(B)). There was no significant difference between the CD68+ population and CD163+ population in either the D-muscle or the D-fascia groups (Figure 8(D)). Compared to D-muscle before implantation (Figure 3(A)), subcutaneously implanted D-muscle underwent remodeling, with new tissue filling in porous space in D-muscle (Figure 8(C)). In the remodeled area, muscle regeneration (MyoD1+ staining) and neovascularization (CD31+) were observed (Figure 8(C)), indicating the potential for applying D-muscle for muscle tissue regeneration. Little remodeling was observed in subcutaneously implanted D-fascia samples: fewer MyoD1+ cells and fewer vascular structures were observed in implanted D-fascia samples than D-muscle samples (Figure 8(C) and (D)).

D-muscle was selected to repair muscle defects created in Fischer 344 rats. On day 30, samples from both groups were harvested and analyzed using immunohistochemical staining. H&E results showed implanted D-muscle underwent remodeling and bridged the muscle defect (Figure 9(A)). In the non-repaired muscle defect group, muscle defect remained and a capsule composed of connective tissue was observed covering the native muscle tissues (Figure 9(B)). While in repaired group, the muscle defect was filled with remodeled D-muscle, which was composed of both connective tissue and regenerative muscle tissue (Figure 9(B) and (C)). MyoD1+ cells were observed uniformly distributed within D-muscle at the muscle defect site of repaired group, whereas few MyoD1+ cells were observed at the muscle defect site of non-repaired group (Figure 9(C)).

4. Discussion

Decellularization is a technique that can be applied to remove cellular components and maintain native ECM structure and properties [7]. Physical, chemical, and enzymatic methods have been applied in the decellularization process. Methods used in the process inevitably affected the resultant ECM scaffold properties to some extent [23]. In this study, we followed the basic rules of decellularization and developed a protocol for musculofascial tissue decellularization in order to avoid harsh changes to native ECM properties. Our results show that this protocol is efficient for removing cellular components from muscle or fascia tissues. Only a little nuclear debris was observed in D-muscle or D-fascia, which may be due to a small amount of cell nuclear material sticking in D-muscle or D-fascia scaffolds. Large-molecular-weight DNA may cause a severe host immune reaction, which may lead to immunorejection of implanted materials [24, 25]. Even though a small amount of small-molecular-weight DNA may not cause implant failure, we are still investigating how to completely remove DNA from D-muscle and D-fascia to achieve 100% safety.

Improvements to the current protocol include modifying the DNase dissolved buffer to optimize DNase's activity (data not shown). In addition to pig musculofascial tissue, we have successfully applied this new protocol to decellularize human adipose tissue, as well as rat soft tissue, such as muscle, skin, and blood vessels, with achievement of complete removal of cells in ECM (data not shown). These data indicate that the protocol used in the present study is of advantage for soft tissue acellularization. After decellularization, the native ECM structure was well maintained in both D-muscle and D-fascia samples. The resultant ECM architecture of D-muscle samples presented microporous and nanofibrous hybrid structures. The 3D architecture of D-fascia was similar to native fascial tissue except that no cells were observed in D-fascia samples. Compared with other studies that only showed micro-porous structures in resultant D-muscle samples [23, 26], the protocol used in this study better maintained the native ECM structure and provided more detailed and accurate information about native ECM architecture of muscle tissues. Even though GAG could be affected during the decellularization process, GAG content was still measurable in D-muscle and D-fascia.

While D-muscle and D-fascia showed lots of similarities, both own different characteristics in some aspects. After removal of cellular components in muscle tissue or fascial tissue, D-muscle and D-fascia still presented strong mechanical properties. D-fascia showed stronger UTS and E than D-muscle, while D-muscle showed higher strain at failure than D-fascia. These results are consistent with functions of native muscle tissues and fascial tissues. Native fascia and muscles provide strong tensile strength, while native muscles also provide flexibility *in vivo*. D-muscle and D-fascia were primarily composed of collagen and laminin. Collagen is a major component of most tissues. Laminin functions to improve cell adhesion and function *in vivo*. In D-muscle samples, collagen formed a layered structure surrounding multiple muscle cell bundles, while laminin formed a microporous structure that was distributed along single muscle cell bundles. In D-fascia samples, collagen formed bundles that formed the major structure of fascial ECM, while laminin formed nanofibrous meshes among these collagen bundles. To better mimic the native muscle ECM properties with respect to components, collagen and laminin can form the major scaffold. In addition to the component aspect, biologic scaffold design for musculofascial tissue regeneration should include micro- and nanostructures. Constructs with different layers of structures with feature size ranging from microscale to nanoscale would be a promising design to mimic natural musculofascial structure.

One important growth factor, VEGF was also observed in D-muscle and D-fascia ECM. In D-muscle samples, abundant VEGF distributed along nanofibrous structures surrounding cells. However, only a small amount of positive staining for VEGF was observed in native fascia tissues and D-fascia tissues. These results indicated that muscle tissue is rich in VEGF. The observation of growth factors (e.g. VEGF) on DMM suggests that DMM may possess pro-angiogenic properties; this hypothesis was further confirmed with the aortic ring assay to test the bioactivity of preserved VEGF in D-muscle and D-fascia. In the aortic ring samples treated with D-muscle-conditioned media, cells migrated further than those in the control group, and vessel branches were formed in collagen gel. In contrast, in the aortic ring samples treated with D-fascia-conditioned media, cells migrated further than both the

control group and D-muscle-conditioned media, but fewer vessel branches were observed in this group. These results suggest that some other growth factors that could promote cell migration may exist in D-fascia samples. For example, canine skeletal muscle ECM was shown to contain bFGF [19]. Further work on characterization of preserved growth factors is needed to gain a better understanding of the pig DMM system. Preservation of biologically functional growth factors in DMM would benefit cell proliferation and vascularization after transplantation *in vivo*, which would benefit graft host integration, remodeling, and final survival [27].

The combination of scaffolds and stem cells holds great promise in tissue engineering [2, 5]. hASCs have been shown as a promising cell source for tissue regeneration owing to their wide availability, stem cell properties, and absence of ethical issues. To apply D-muscle and D-fascia in musculofascial engineering in the presence of hASCs, biocompatibility of the scaffold with hASCs was important. In this study, hASCs were successfully integrated with D-muscle and D-fascia and those cells established adhesion, proliferated, elongated, and formed aligned patterns in long-time culture (e.g. 7 days). These results indicated both D-muscle and D-fascia provided a compatible and supportive environment for recellularization.

To test the implant-host interaction, D-muscle and D-fascia were transplanted in rat. Heterotopic implantation of D-muscle and D-fascia did not result in any signs of allograft rejection. However, implanted D-muscle and D-fascia scaffolds did elicit a foreign-body response as shown by macrophage infiltration (CD68+ cells). This observation is consistent with other reports [18–19]. Abundant CD45+ macrophages and granulocytes have been shown in the acellular mice muscle scaffold after implantation in the mice model [18]. The decellularized canine muscle ECM also showed a robust mononuclear cell response in a rat model [19]. Unlike a severe foreign-body reaction that results in structural weakening or rapid degradation with severe fibrosis [28], in our study macrophages present within implants are almost at a remodeling stage (CD163+ cells of M2 profile) but not an inflammation stage (CD80+ cells of M1 profile) [25]. In addition, infiltrated cells showed regenerative capacity by staining MyoD1 positive and CD31 positive after D-muscle and D-fascia implantation. More MyoD1+ cells and vessel structures were observed in D-muscle implantation than in D-fascia, which indicates the potential of a D-muscle scaffold for muscle regeneration. This hypothesis was further supported by orthotopic transplanted D-muscle for muscle defect repair with promising results. D-muscle was remodeled with the presence of MyoD1+ cells and muscle fiber-like structures. In the present study, only one time point (i.e. 30 days) was included. Further study over longer periods of time is necessary to evaluate myogenesis when remodeling is complete [19]. To translate to clinical application, composites of D-muscle and D-fascia should be tested in large animal models (such as pig models) to gain a comprehensive understanding of DMM remodeling process.

This study treats muscle and fascia together as a basic unit to represent musculofascial tissues. ECM properties of native musculofascia were examined in D-muscle and D-fascia through the decellularization approach. It is impossible to study deep fascia by using a small animal model, as reported before, due to its weak structure in rodents [17–19]. The few studies about D-muscle derived from a large animal skeletal muscle tissue resource only

focused on the muscle component [19, 20]. Our study provides new insight into the ECM properties of muscle and fascia, both of which are important components of the functional skeletal musculofascial tissues. Property differences (e.g. 3D structures, molecular compositions, mechanical features and pro-angiogenic characters) in D-muscle and D-fascia samples imply that scaffold design for engineering muscle tissue or fascia tissue may take different strategies to mimic the *in vivo* scenario. Properties differences in D-muscle and D-fascia scaffolds also indicate their different applications if used alone. For example, skeletal muscle has been utilized as a nerve conduit [9]. D-muscle may provide an alternative to skeletal muscles derived from patients to avoid intrusion injury with more and easier access. Another possible application of D-muscle is for dead space filling and soft tissue augmentation in reconstructive surgery, which currently uses a lot of adipose tissue as filling materials. In the clinic, deep fascia has been applied to repair tendon defects and soft tissue lift. D-fascia, presenting similarity to tendons in mechanical properties and structural features, could be applied as an alternative material for soft tissue lift and tendon repair [15, 29], which could reduce the cost and pain caused by additional surgery. Further, DMM from pig tissue resources, used alone or recellularized, has tremendous clinically-translatable potential. For example, musculofascial tissues defect caused by tumor removal may lead to hernia. Lots of biomaterials have been developed to repair hernias in clinic (e.g. porcine acellular dermal matrix, polypropylene meshes) [10, 14]. However, there are still no perfect implants to induce muscle regeneration and effectively prevent hernia recurrence. Based on the present study, D-muscle scaffold represents a pro-angiogenic and pro-myogenic environment, while D-fascia provides important mechanical support. Being consistent with the plastic rule that “replace with alike”, DMM comprising muscle and fascia ECM as a whole unit could provide a natural platform for musculofascial tissue repair and regeneration.

5. Conclusions

This study showed the detailed characterization of decellularized pig musculofascial matrix. Resultant D-muscle and D-fascia presented effective cellular component removal, a well-maintained 3D architecture, strong mechanical properties and biochemical components. D-muscle and D-fascia were non-cytotoxic and affected hASC integration with respect to cell morphology and integrin binding, which indicates a carrier for stem cell-based therapy by providing an *in-vivo* mimetic niche. *In vitro* aortic ring assay demonstrated that D-muscle possessed strong pro-angiogenic properties. Heterotopic and orthotopic implantation of D-muscle and D-fascia in a rodent model further proved their biocompatibility and myogenic properties during the remodeling process, showing their regenerative capacity for musculofascia repair. The differing characteristics of D-muscle from D-fascia (e.g., D-muscle’s strong pro-angiogenic and pro-myogenic properties vs. D-fascia’s strong mechanical properties) indicate different clinical application opportunities of D-muscle vs. D-fascia scaffolds. In conclusion, decellularized pig musculofascial matrix, comprising of muscle and fascia ECM as a whole unit, can thus provide not only a clinical translatable platform for musculofascial tissue repair and regeneration, but also a useful standard for scaffold design in musculofascial tissue engineering.

Supplementary Material

Refer to Web version on PubMed Central for supplementary material.

Acknowledgments

This study is supported by a grant from the Kyte Foundation through the Department of Plastic Surgery of The University of Texas MD Anderson Cancer Center (Q. Zhang). We thank the High Resolution Electron Microscopy Facility (NIH Cancer Center Core Grant P30CA016672) for SEM imaging and the Flow Cytometry and Cellular Imaging Core Facility for confocal imaging.

References

1. Badylak SF, Weiss DJ, Caplan A, Macchiarini P. Engineered whole organs and complex tissues. Lancet. 2012; 379(9819):943–952. [PubMed: 22405797]
2. Deans TL, Elisseeff JH. Stem cells in musculoskeletal engineered tissue. Curr Opin Biotechnol. 2009; 20(5):537–544. [PubMed: 19879127]
3. Ma J, Holden K, Zhu J, Pan H, Li Y. The application of three-dimensional collagen-scaffolds seeded with myoblasts to repair skeletal muscle defects. J Biomed Biotechnol. 2011; 2011:812135. [PubMed: 22203786]
4. Merritt EK, Hammers DW, Tierney M, Suggs LJ, Walters TJ, Farrar RP. Functional assessment of skeletal muscle regeneration utilizing homologous extracellular matrix as scaffolding. Tissue Eng Part A. 2010; 16(4):1395–1405. [PubMed: 19929169]
5. Rossi CA, Pozzobon M, De Coppi P. Advances in musculoskeletal tissue engineering: moving towards therapy. Organogenesis. 2010; 6(3):167–172. [PubMed: 21197219]
6. Page RL, Malcuit C, Vilner L, Vojtic I, Shaw S, Hedblom E, et al. Restoration of skeletal muscle defects with adult human cells delivered on fibrin microthreads. Tissue Eng Part A. 2011; 17(21–22):2629–2640. [PubMed: 21699414]
7. Badylak SF, Freytes DO, Gilbert TW. Extracellular matrix as a biological scaffold material: Structure and function. Acta Biomater. 2009; 5(1):1–13. [PubMed: 18938117]
8. Moore AM, MacEwan M, Santosa KB, Chenard KE, Ray WZ, Hunter DA, et al. Acellular nerve allografts in peripheral nerve regeneration: a comparative study. Muscle Nerve. 2011; 44(2):221–234. [PubMed: 21660979]
9. Zhang XY, Xue H, Liu JM, Chen D. Chemically extracted acellular muscle: a new potential scaffold for spinal cord injury repair. J Biomed Mater Res A. 2012; 100(3):578–587. [PubMed: 22213649]
10. Butler CE, Burns NK, Campbell KT, Mathur AB, Jaffari MV, Rios CN. Comparison of cross-linked and non-cross-linked porcine acellular dermal matrices for ventral hernia repair. J Am Coll Surg. 2010; 211(3):368–376. [PubMed: 20800194]
11. Gilbert TW, Sellaro TL, Badylak SF. Decellularization of tissues and organs. Biomaterials. 2006; 27(19):3675–3683. [PubMed: 16519932]
12. Seif-Naraghi SB, Salvatore MA, Schup-Magoffin PJ, Hu DP, Christman KL. Design and characterization of an injectable pericardial matrix gel: a potentially autologous scaffold for cardiac tissue engineering. Tissue Eng Part A. 2010; 16(6):2017–2027. [PubMed: 20100033]
13. Hudson TW, Liu SY, Schmidt CE. Engineering an improved acellular nerve graft via optimized chemical processing. Tissue Eng. 2004; 10(9–10):1346–1358. [PubMed: 15588395]
14. Burns NK, Jaffari MV, Rios CN, Mathur AB, Butler CE. Non-cross-linked porcine acellular dermal matrices for abdominal wall reconstruction. Plast Reconstr Surg. 2010; 125(1):167–176. [PubMed: 19910855]
15. Zhang X, Bogdanowicz D, Erisken C, Lee NM, Lu HH. Biomimetic scaffold design for functional and integrative tendon repair. J Shoulder Elbow Surg. 2012; 21(2):266–277. [PubMed: 22244070]
16. Flynn LE. The use of decellularized adipose tissue to provide an inductive microenvironment for the adipogenic differentiation of human adipose-derived stem cells. Biomaterials. 2010; 31(17):4715–4724. [PubMed: 20304481]

17. Stern MM, Myers RL, Hammam N, Stern KA, Eberli D, Kritchevsky SB, et al. The influence of extracellular matrix derived from skeletal muscle tissue on the proliferation and differentiation of myogenic progenitor cells ex vivo. Biomaterials. 2009; 30(12):2393–2399. [PubMed: 19168212]
18. Perniconi B, Costa A, Aulino P, Teodori L, Adamo S, Coletti D. The pro-myogenic environment provided by whole organ scale acellular scaffolds from skeletal muscle. Biomaterials. 2011; 32(31):7870–7882. [PubMed: 21802724]
19. Wolf MT, Daly KA, Reing JE, Badylak SF. Biologic scaffold composed of skeletal muscle extracellular matrix. Biomaterials. 2012; 33(10):2916–2925. [PubMed: 22264525]
20. DeQuach JA, Lin JE, Cam C, Hu D, Salvatore MA, Sheikh F, et al. Injectable skeletal muscle matrix hydrogel promotes neovascularization and muscle cell infiltration in a hindlimb ischemia model. Eur Cell Mater. 2012; 23:400–412. discussion 12. [PubMed: 22665162]
21. Go RS, Owen WG. The rat aortic ring assay for in vitro study of angiogenesis. Methods Mol Med. 2003; 85:59–64. [PubMed: 12710197]
22. Nicosia RF, Ottinetti A. Growth of microvessels in serum-free matrix culture of rat aorta. A quantitative assay of angiogenesis in vitro. Lab Invest. 1990; 63(1):115–122. [PubMed: 1695694]
23. Gillies AR, Smith LR, Lieber RL, Varghese S. Method for decellularizing skeletal muscle without detergents or proteolytic enzymes. Tissue Eng Part C Methods. 2011; 17(4):383–389. [PubMed: 20973753]
24. Gilbert TW, Freund JM, Badylak SF. Quantification of DNA in biologic scaffold materials. J Surg Res. 2009; 152(1):135–139. [PubMed: 18619621]
25. Keane TJ, Londono R, Turner NJ, Badylak SF. Consequences of ineffective decellularization of biologic scaffolds on the host response. Biomaterials. 2012; 33(6):1771–1781. [PubMed: 22137126]
26. Borschel GH, Dennis RG, Kuzon WM Jr. Contractile skeletal muscle tissue-engineered on an acellular scaffold. Plast Reconstr Surg. 2004; 113(2):595–602. discussion 3–4. [PubMed: 14758222]
27. Murphy WL. Temporal and spatial control over soluble protein signaling for musculoskeletal tissue engineering. Conf Proc IEEE Eng Med Biol Soc. 2009; 2009:2103–2105. [PubMed: 19964780]
28. Moyer AL, Wagner KR. Regeneration versus fibrosis in skeletal muscle. Curr Opin Rheumatol. 2011; 23(6):568–573. [PubMed: 21934499]
29. Turner NJ, Yates AJ Jr, Weber DJ, Qureshi IR, Stolz DB, Gilbert TW, et al. Xenogeneic extracellular matrix as an inductive scaffold for regeneration of a functioning musculotendinous junction. Tissue Eng Part A. 2010; 16(11):3309–3317. [PubMed: 20528669]

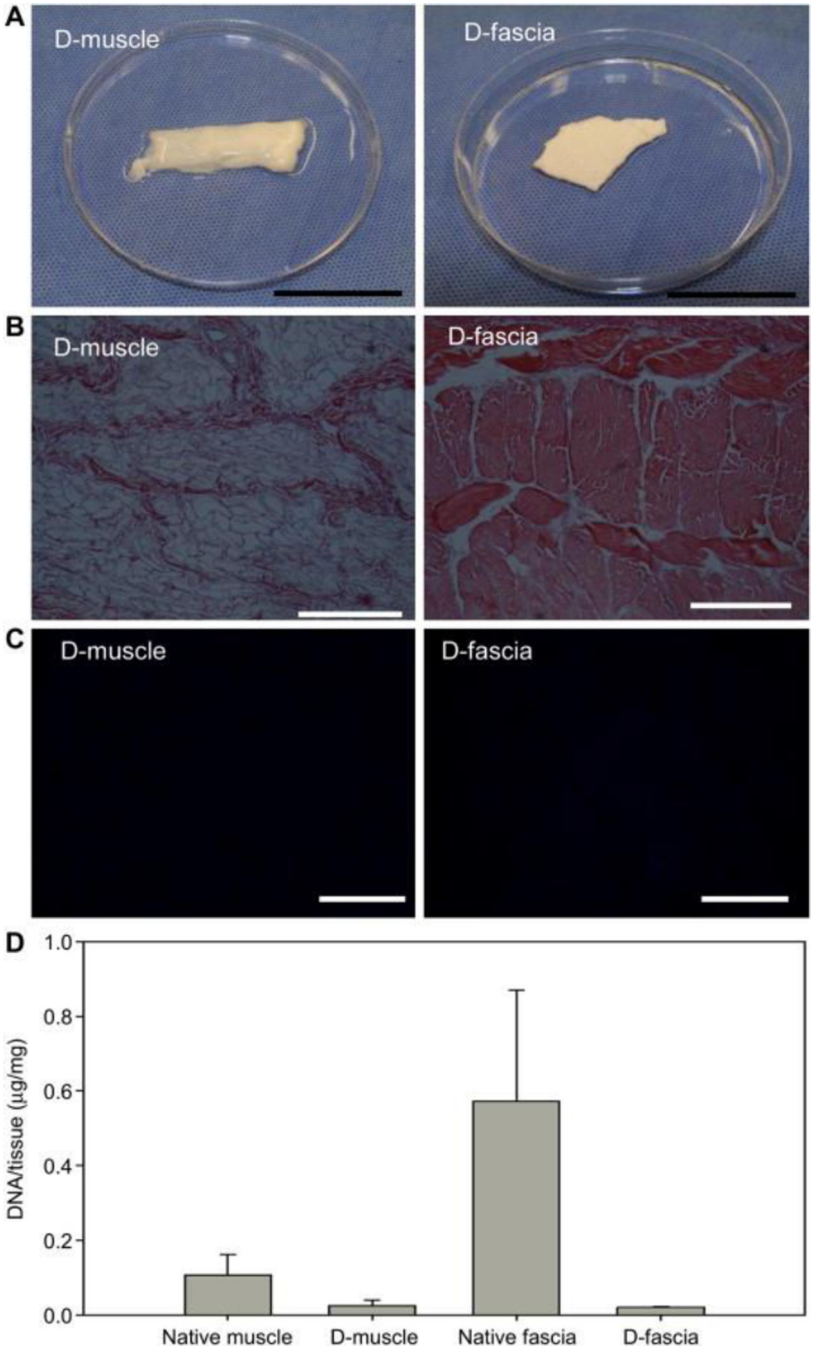

Figure 1.

Evaluation of cellular components' removal from musculofascial tissues. (A) Images of muscle and fascial tissue after decellularization. (B) H&E staining of decellularized samples (D-muscle and D-fascia). (C) DAPI staining decellularized samples. (D) DNA content in dry weight samples. Scale bar = 20 mm in (A), 200 μm in (B) and (C).

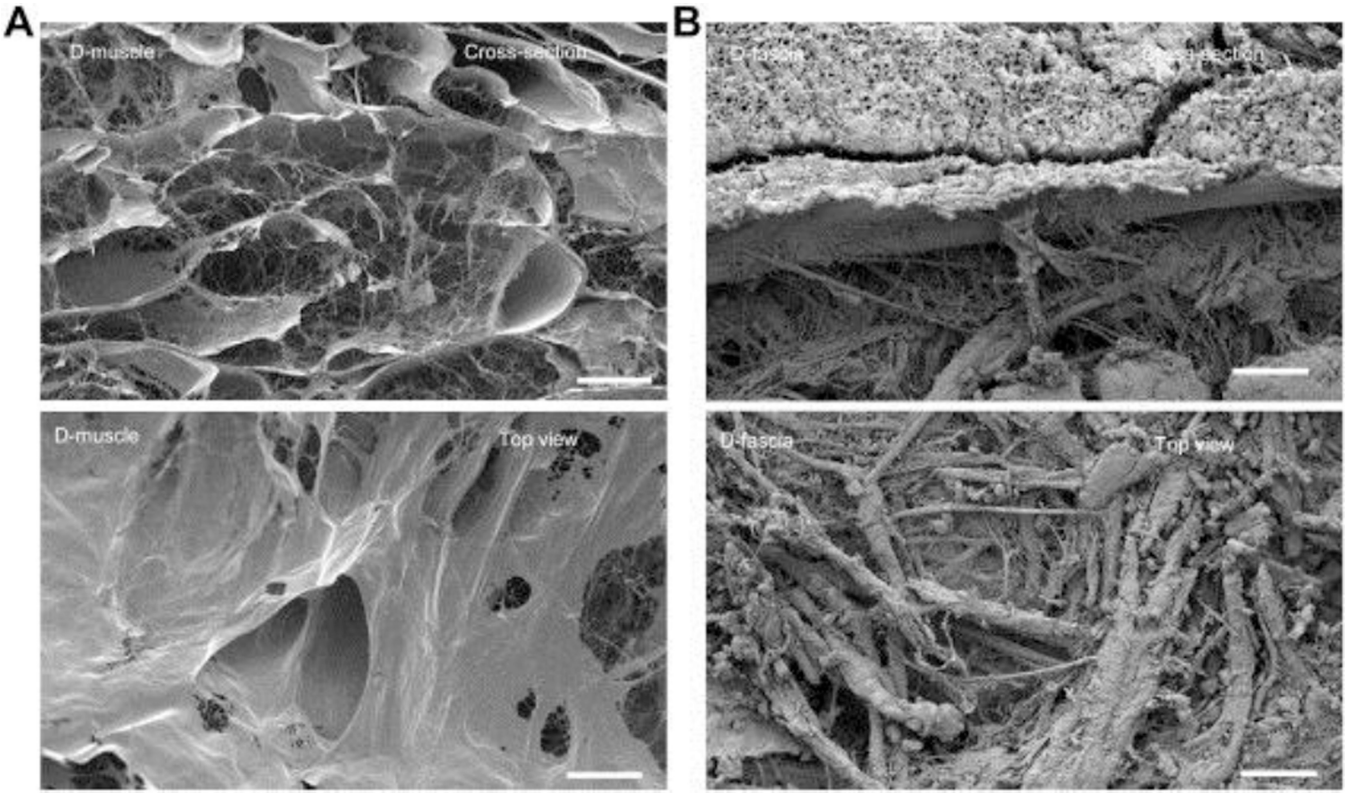

Figure 2.

SEM images of D-muscle (A) and D-fascia (B). The top row in each image shows the cross-sectional view, the bottom row shows the top view. Scale bar = 50 μm.

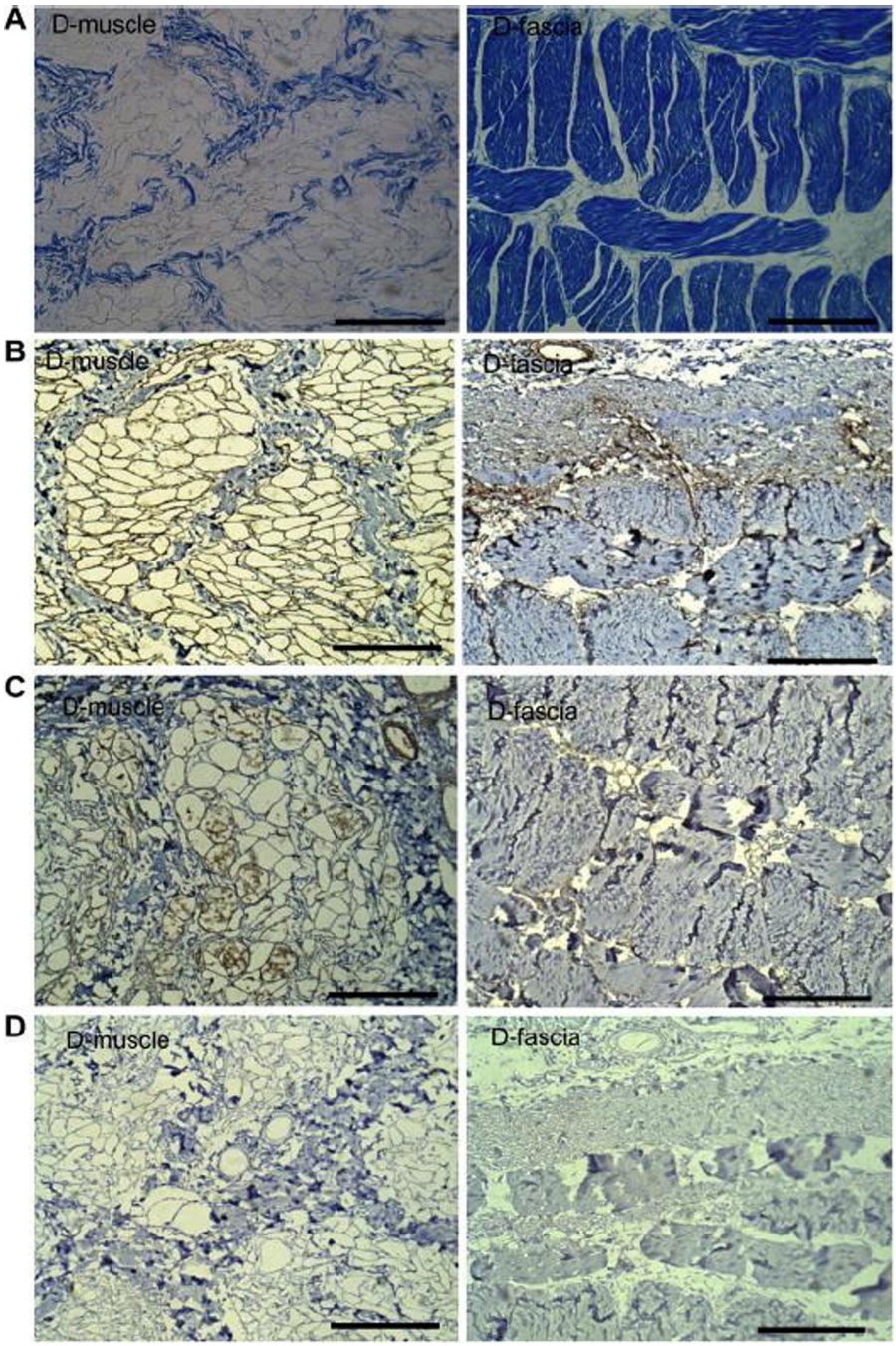

Figure 3.

Characterization of D-muscle and D-fascia components. (A) Masson Trichrome staining shows the major structures of D-muscle and D-fascia are composed of collagen. (B) Laminin staining shows that after decellularization the fibrous structures among collagen structures are stained positively for laminin. Similar laminin distribution was noticed in D-fascia. (C) VEGF staining shows VEGF is retained in the nanofibrous structures within these small tubular structures in D-muscle. In D-fascia, VEGF staining was weakly positive

in limited areas among collagen bundles (e.g. around blood vessels). (D) MHC-1 staining shows negative results in D-muscle and D-fascia. Scale bar = 200 μm.

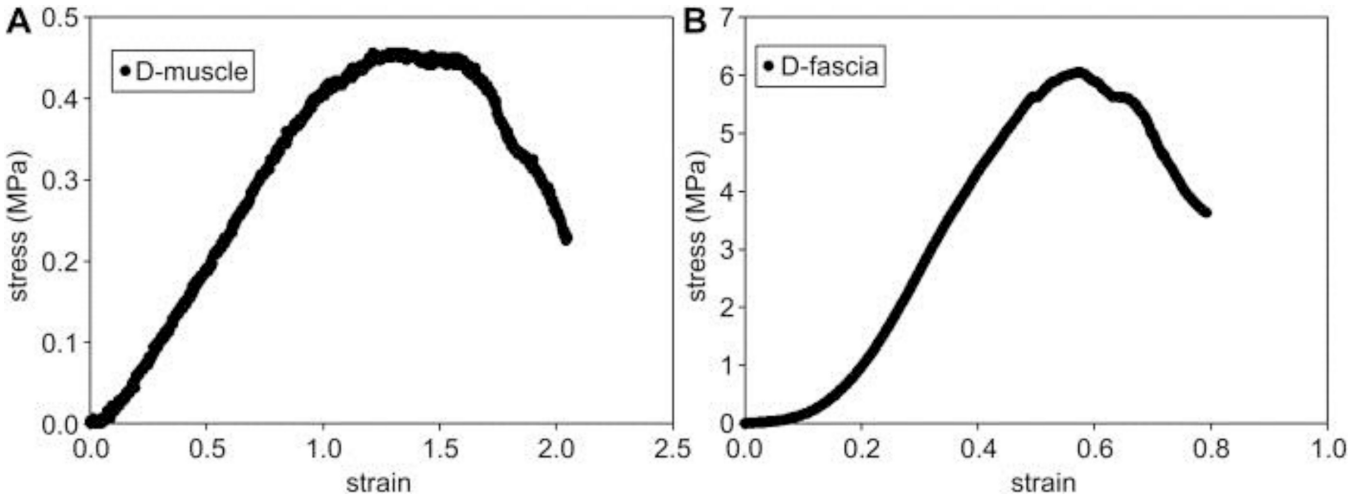

Figure 4.

Typical strain-stress curves of D-muscle (A) and D-fascia (B) measured by uniaxial tensile testing.

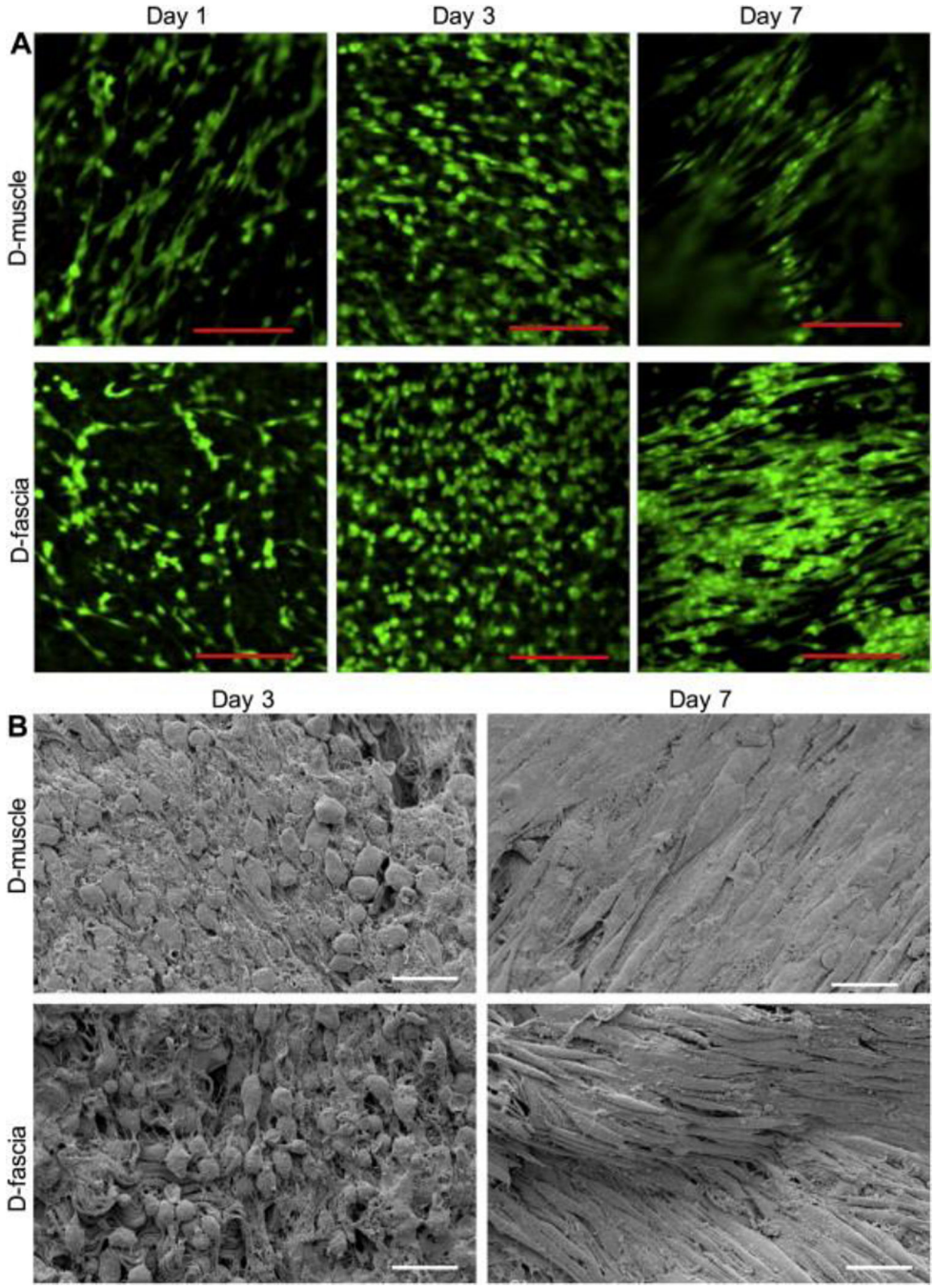

Figure 5.

(A) Confocal images showing ASCs on D-muscle and D-fascia samples. ASCs were stained with Calcein AM on days 1, 3, and 7 after plating. (B) SEM images showing ASCs on D-muscle and D-fascia on days 3 and day 7 after integration. Scale bar = 100 μm in (A) and 50 μm in (B).

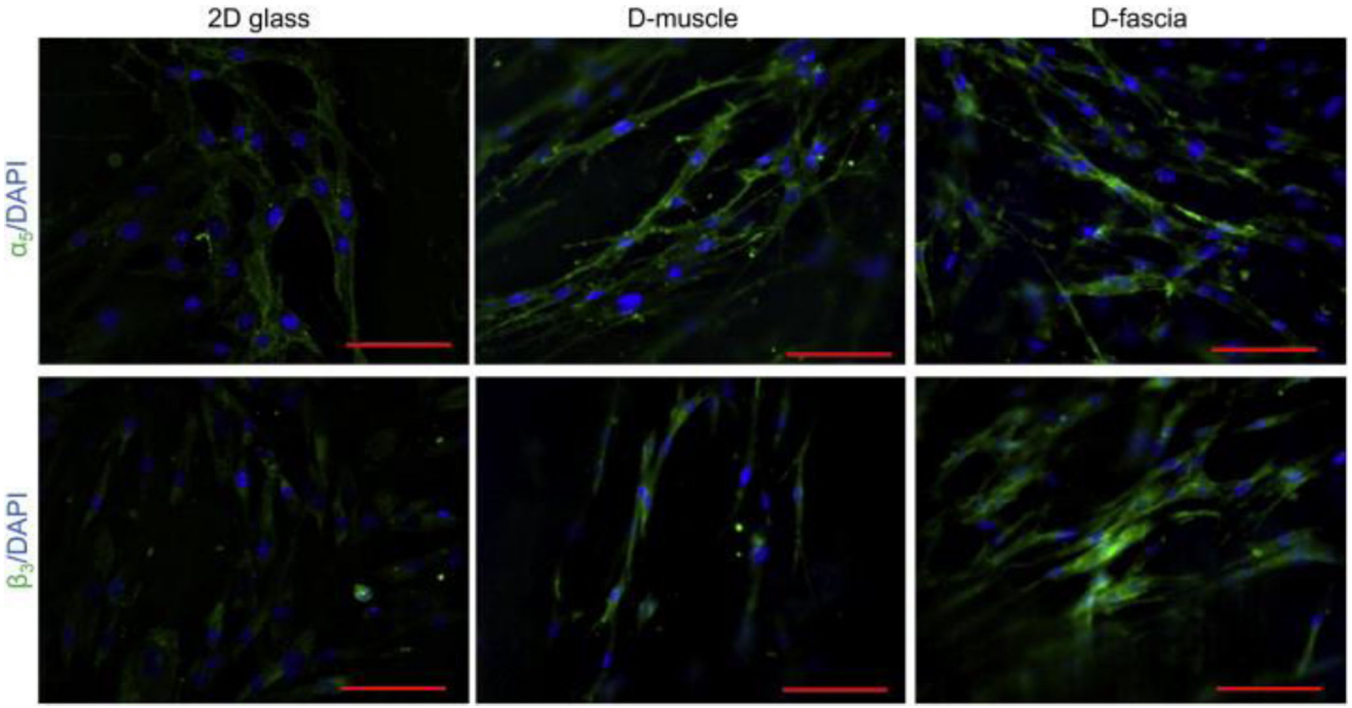

Figure 6.

Confocal images showing ASCs on 2D glass slides, D-muscle, and D-fascia samples. ASCs were stained for integrin α_5 or β_3 (green) and DAPI (blue). Scale bar = 100 μm.

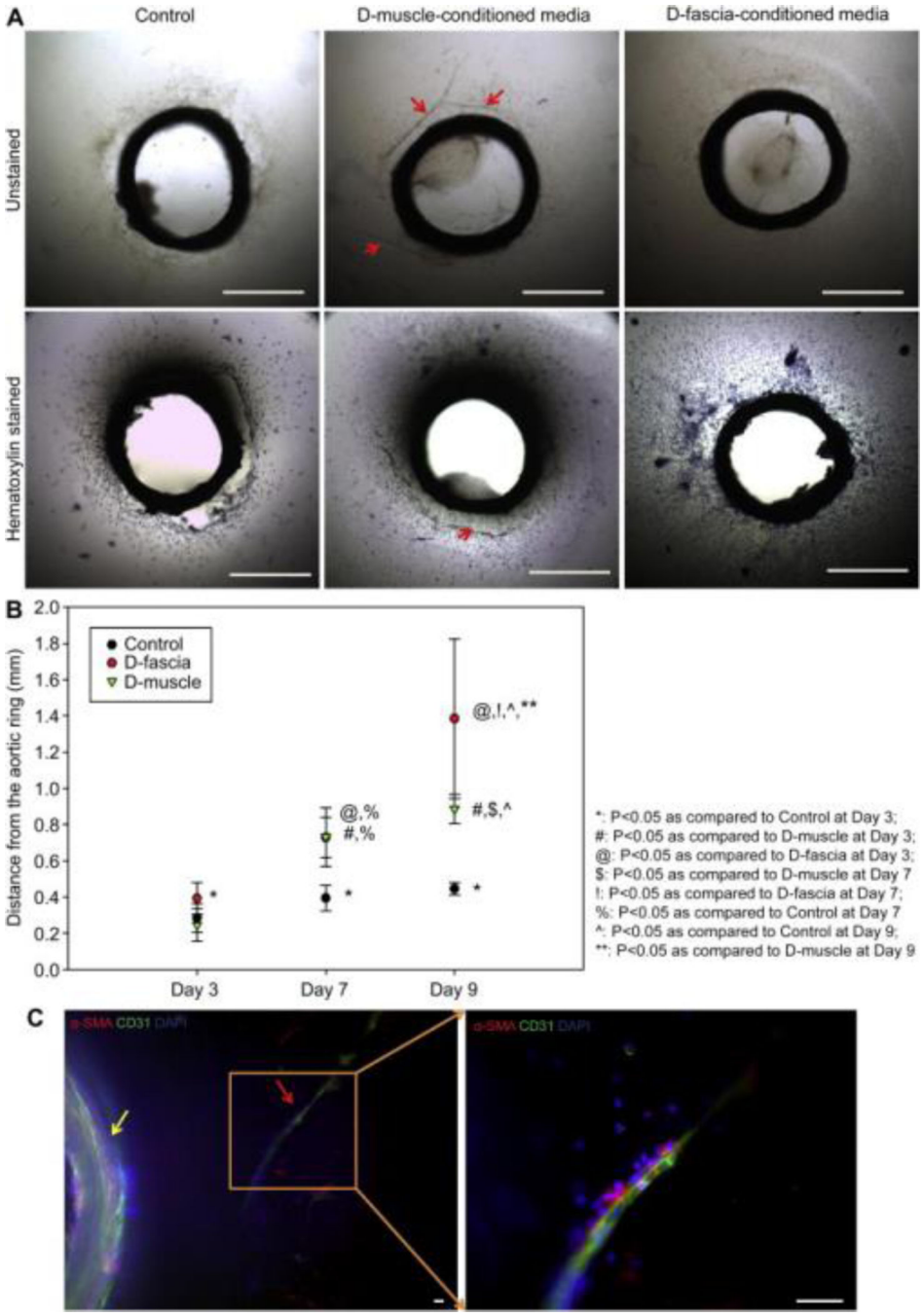

Figure 7.

Aortic ring assay with D-muscle-conditioned media and D-fascia-conditioned media. (A) Phase contrast images of aortic rings on day 7 of *in vitro* cultures treated with control media (EGM media), D-muscle-conditioned media, and D-fascia-conditioned media. Samples were also stained with hematoxylin and imaged. Vessel branch outgrowth (as indicated by the red arrow) from the aortic ring in 3D collagen gel was observed on day 7 of *in vitro* culture treated with D-muscle-conditioned media. (B) Cell migration distance from the aortic ring measured on days 3, 7, and 9 of *in vitro* cultures treated with control media (EGM media),

D-muscle-conditioned media, and D-fascia-conditioned media. (C) Confocal images showing vessel branch outgrowth (as indicated by the red arrow) from the aortic ring (as indicated by the yellow arrow) in 3D collagen gel on day 7 of *in vitro* culture treated with D-muscle-conditioned media. Samples were stained for α-smooth muscle actin (α-SMA, red), CD31 (green), and DAPI (blue). Scale bar = 1 mm in (A) and 50 μm in (C).

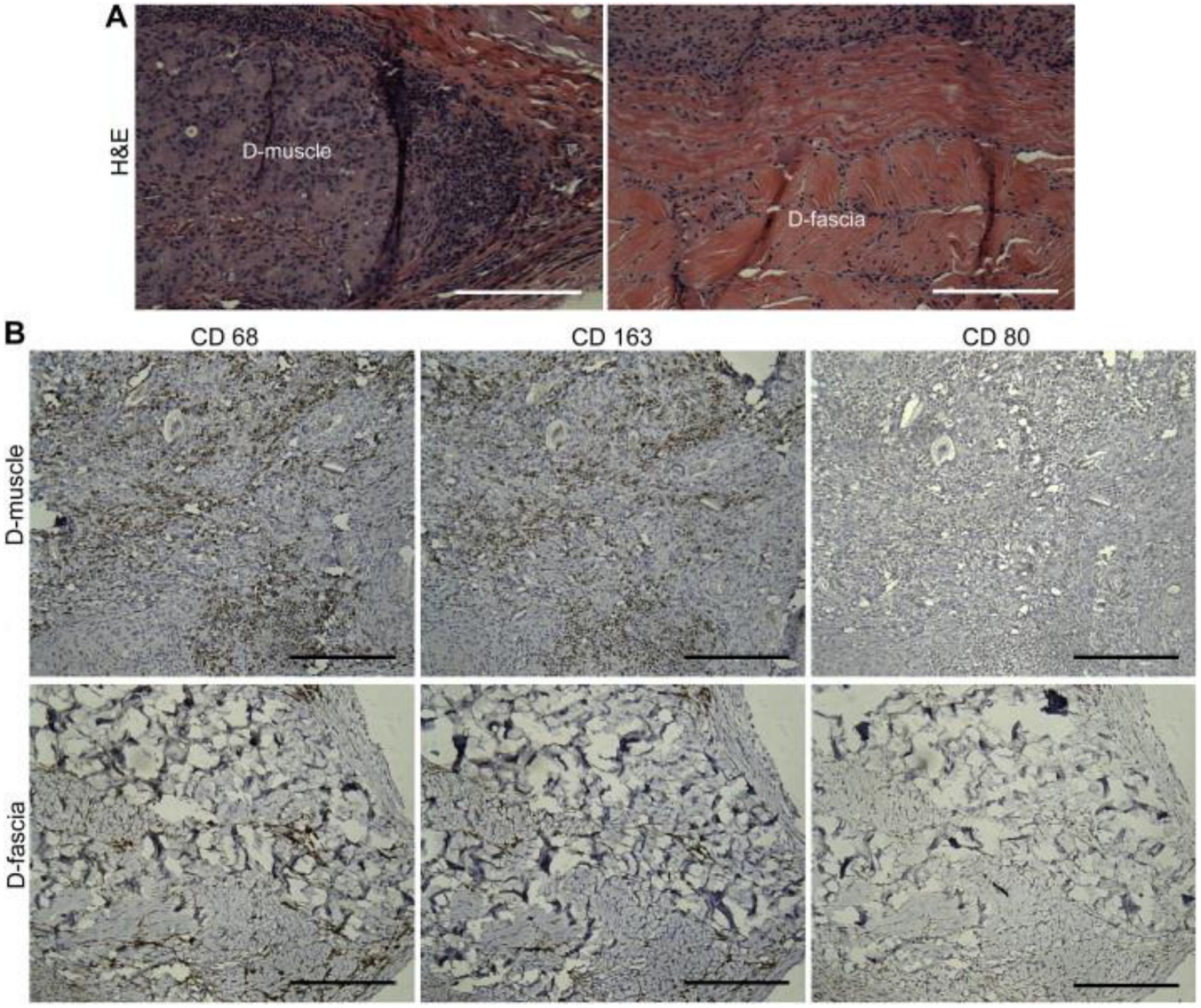

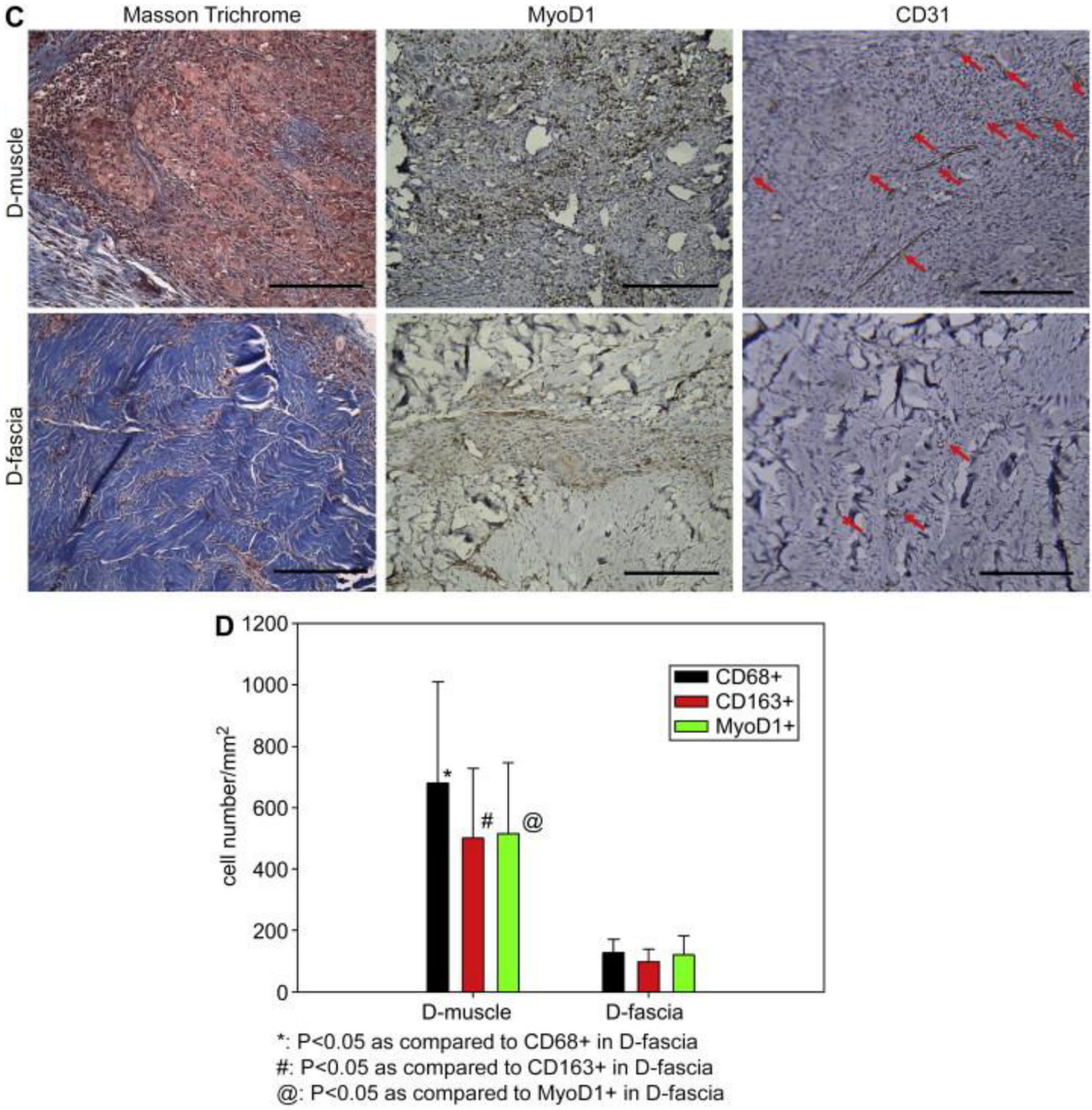

Figure 8.

(A–C) Immunohistochemical staining of D-muscle and D-fascia 30 days after subcutaneous implantation in Fischer 344 rats. (A) H&E staining. (B) Staining for CD68, CD163, CD 80. (C) Masson Trichrome, MyoD1 and CD31 staining. Scale bar = 200 μm. (D) Summary of cell density (cells/mm^2) of cells that stained positively for CD68, CD163 and MyoD1.

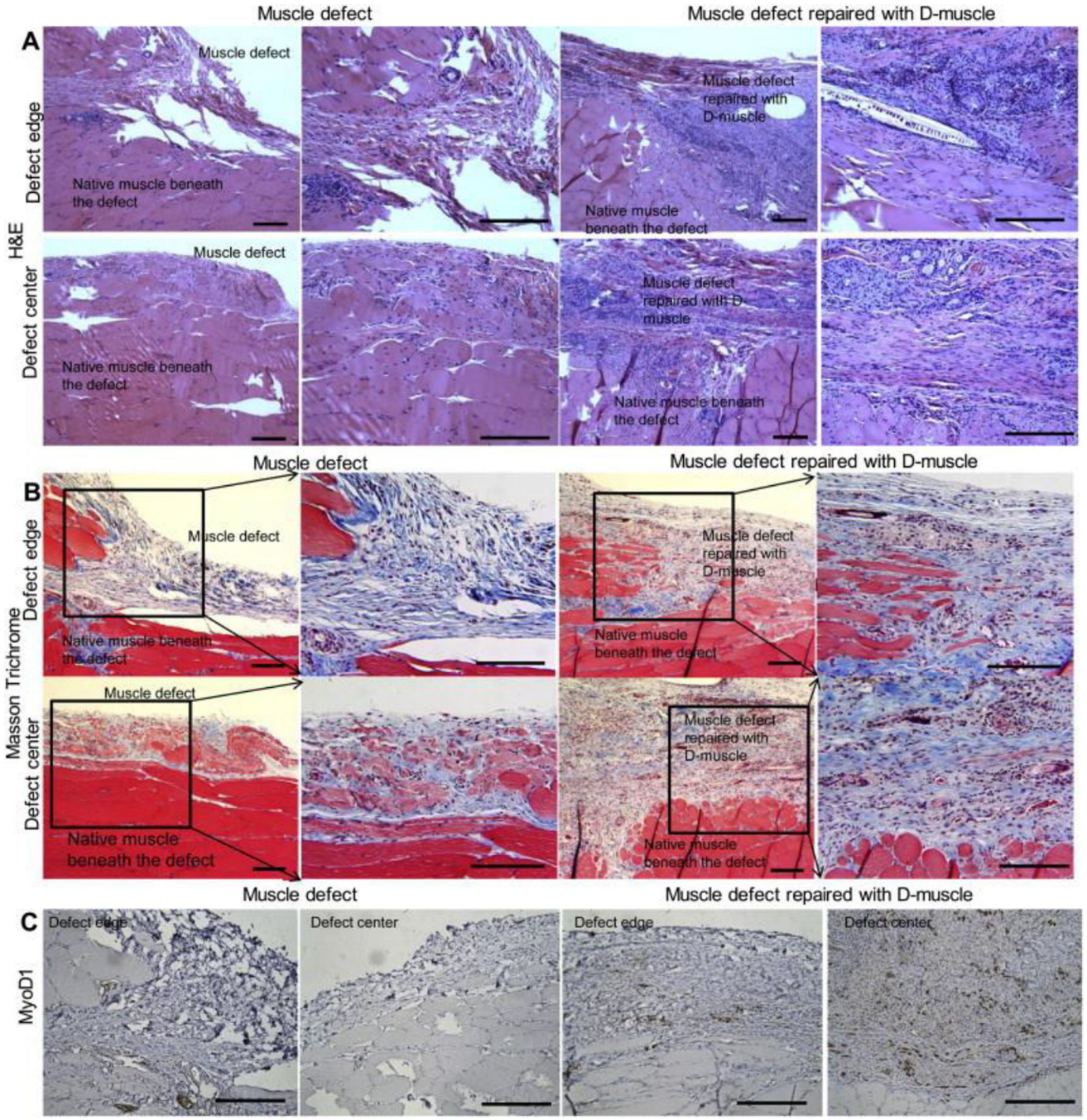

Figure 9.

Immunohistochemical staining of muscle defect without repair and defect repaired with D-muscle on day 30 after surgery. (A) H&E staining. (B) Massion Trichrome staining. (C) MyoD1 staining. Scale bar = 200 μm.

Table 1

Mechanical properties measured from stress-strain curves obtained via uniaxial tensile test [*]

	Fascia		Muscle	
	Native fascia (n = 6)	**D-fascia (n = 6)**	**Native muscle (n = 6)**	**D-muscle (n = 6)**
UTS (MPa)	3.47±0.48[!]	4.02±1.49[#]	0.21±0.08[##]	1.32±0.85
E (MPa)	11.66±2.87[$]	8.15±4.96[@]	0.19±0.07	0.41±0.32
Strain at failure	0.43±0.15[^%]	0.65±0.19[&]	1.24±0.27[&&]	1.60±0.30

Abbreviations: UTS, ultimate tensile strength; E, elastic modulus; D-fascia: decellularized fascia; D-muscle: decellularized muscle.

[*] Values reported as mean ± standard deviation

[#] P<0.05 as compared to D-muscle for UTS

[@] P<0.05 as compared to D-muscle for E

[&] P<0.05 as compared to D-muscle for strain at failure

[!] P<0.05 as compared to native muscle for UTS

[$] P<0.05 as compared to native muscle for E

[%] P<0.05 as compared to native muscle for strain at failure

[^] P<0.05 as compared to D-fascia for strain at failure

[##] P<0.05 as compared to D-muscle for UTS

[&&] P<0.05 as compared to D-muscle for strain at failure

Table 2

Summarization of cellular morphology on DMM samples on day 3 and day 7 in culture.

	D-muscle				D-fascia			
	Area (um2) (mean±SD)	**Perimeter (um) (mean±SD)**	**Elongation (mean±SD)**	**Roundness (mean±SD)**	**Area (um2) (mean±SD)**	**Perimeter (um) (mean±SD)**	**Elongation (mean±SD)**	**Roundness (mean±SD)**
Day 3	275.0±92.5 (n=55)	71.7±6.8 (n=55)	2.3±1.3 (n=55)	0.7±0.1 (n=55)	225.2±76.1 (n=31) #	62.2±15.3 (n=31)#	1.9±1.1 (n=31)	0.7±0.1 (n=31)#
Day 7	697.5±215.9 (n=17)*	183.8±46.0 (n=17)*	10.7±5.0 (n=17)*	0.3±0.1 (n=17)*	592.5±250.8 (n=33)*	184.2±50.8 (n=33)*	13.0±4.3 (n=33)*	0.2±0.1 (n=33)* @

*P<0.05 as compared day 3

#P<0.05 as compared to D-muscle at day 3

@P<0.05 as compared to D-muscle at day 7